ADVANCED THEORY AND SIMULATIONS
www.advtheorysimul.com

Structural and Electronic Properties of Metal/Oxide Nanostructures from First-Principles: Ru_{13} Supported on $(TiO_2)_{84}$ as a Case Study

*Miquel Allès, Elena R. Remesal, Francesc Illas, and Ángel Morales-García**

All electron density functional theory-based calculations are carried out to investigate the properties of metal/oxide nanostructures taking the case of a Ru_{13} cluster supported on an octahedral anatase $(TiO_2)_{84}$ nanoparticle, as a representative system. The interaction between both systems is exothermic showing binding energies below −4 eV. In spite of the large interaction, the structure of the $(TiO_2)_{84}$ nanoparticle remains unaltered. However, the metal-support interaction promotes the deformation of the Ru_{13} cluster atomic structure. This deformation is more accentuated when the Ru_{13} nanocluster is situated in the facet region of the $(TiO_2)_{84}$ nanoparticle than when the interaction involves the edge regions. The formation of the $Ru_{13}/(TiO_2)_{84}$ heterostructure leads to a decrease of the energy gap inherent to the bare $(TiO_2)_{84}$ nanoparticle, becoming almost negligible. This is due to the contribution of the partially filled Ru 4d orbitals with Kohn–Sham energies spanning in the energy range of those of the O 2p occupied and Ti 3d empty manifolds. This feature is systematically observes no matter the interaction involves the oxide nanoparticle facet or edge regions. This study constitutes a first step in designing a strategy to investigate metal-semiconductor nanostructures using realistic models that go beyond the use of extended surfaces.

1. Introduction

Since 1972, when Fujishima and Honda first reported water splitting with TiO_2 photoelectrodes under UV illumination,[1] this simple oxide has become the workhorse in the field of photocatalysis. Together with its photocatalytic activity,[2,3] low toxicity and cost, high chemical stability are other important features of this semiconductor. However, its restrictive light absorption, requiring UV radiation, and fast recombination limit somehow its use as photocatalyst under sunlight. Therefore, different strategies are being currently investigated with the goal of reducing energy gap and prolonging the lifetime of the photogenerated species. Strategies such as crystal facet engineering, surface modification by supporting metal nanoclusters, and metal/nonmetal doping, to name a few, emerge as plausible procedures to improve the performance of TiO_2 and related semiconducting photocatalysts.[4–8] Among these, the incorporation of metals, typically Pt, Au, or Ru, to semiconducting nanostructures is one of the approaches followed nowadays to enhance the photocatalytic activity of the latter in processes such as water splitting to produce H_2.[9,10] The photocatalytic improvement resides both, the charge separation of the photogenerated electrons and holes and adsorption of visible light. It has been suggested that the charge transfer between semiconductor and metal cluster is important in separating electron–hole pairs.[11,12] This constitutes a great advantage specially for photocatalyst such as titania (TiO_2) where the fast electron–hole recombination is one of the main drawbacks.

Previous experimental studies have reported that the synergy metal cluster and TiO_2 nanocrystals improve the photocatalytic performance with respect to the isolated TiO_2 configuration. Zhang et al.[13] synthetized nanocatalysts of Ag nanoparticles (NPs) coating TiO_2 nanocrystals exposing {101} and {001} facets simultaneously. This Ag/TiO_2 system improves the activation of O_2. Further combined experimental and computational studies confirmed that the adsorption of Pd nanoclusters (NCs) on the TiO_2 NPs reduced the energy activation for the hydrogenation of phenyl acetylene.[14] On the other hand, the photoactivity of TiO_2 has been computationally investigated considering the effect of surface-deposited Pt on the O_2 adsorption.[15] It has been suggested that Pt clusters act as an electron–hole separation center and therefore inhibit the recombination, but that at high loadings Pt acts as an electron–hole recombination center.[16,17] These studies manifest the importance of depositing metal

M. Allès, E. R. Remesal, F. Illas, Á. Morales-García
Departament de Ciència de Materials i Química Física & Institut de Química Teòrica i Computacional (IQTCUB)
Universitat de Barcelona
c/Martí i Franquès 1-11, Barcelona 08028, Spain
E-mail: angel.morales@ub.edu

The ORCID identification number(s) for the author(s) of this article can be found under https://doi.org/10.1002/adts.202200670

DOI: 10.1002/adts.202200670

clusters on TiO_2 but in a controlled way. It is worth noting that, from a theoretical and computational viewpoint, these studies and others[18–20] use periodic models of extended surfaces to analyze the fundamental aspects of the interaction between TiO_2 and metal clusters. These extended surface models represent properly the facets of TiO_2 nanostructures but cannot provide information regarding other region such as edges, apical, or equatorial region that, involving undercoordinated atoms, are likely to be more reactive. To properly investigate the chemistry involved in these regions, realistic TiO_2 NPs are better suited. Thus, computational studies combining metal clusters and realistic TiO_2 NPs are required to provide a more complete picture of the fundamental structural and electronic aspects of these complex heterostructures.

Based on our experience in the analysis of the atomic and electronic structure of realistic TiO_2 NPs including not only the design of particular morphologies but also the study of excited states, hydroxylation, and analysis of doping effects,[21–24] we move a step further to explore here the formation of nanostructures combining Ru_{13} NC with $(TiO_2)_{84}$ NP. The aim of this study is to investigate in detail the interaction of Ru_{13} NC considering the different regions of $(TiO_2)_{84}$ NP and observe the influence on the electronic properties compared with the isolated $(TiO_2)_{84}$ configuration. The paper starts with a brief description of the computational strategy and models. Next, we discuss the binding properties of Ru_{13} NC on the $(TiO_2)_{84}$ NP. Finally, we describe the results of the electronic properties of $Ru_{13}/(TiO_2)_{84}$ systems and outline the main conclusions.

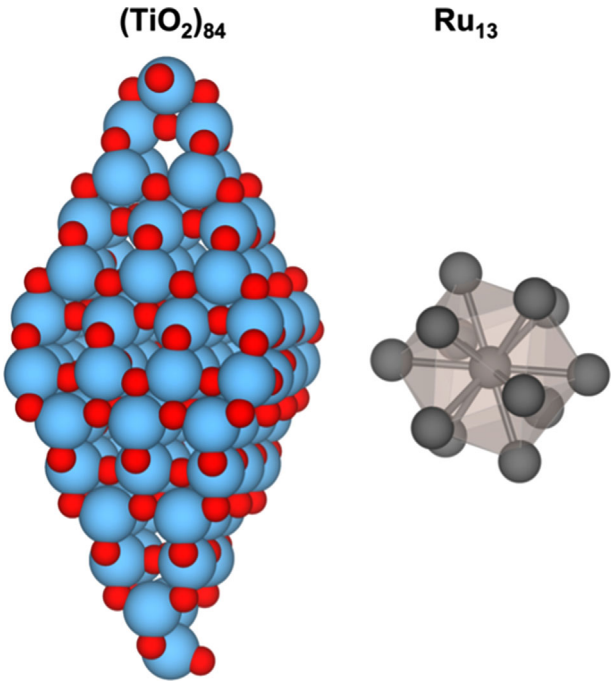

Figure 1. $(TiO_2)_{84}$ and Ru_{13} nanostructures employed in this study. The former has a bipyramidal symmetry and the (101) surface is exposed in all facets. The latter has an icosahedral symmetry. Blue, red, and gray spheres correspond to Ti, O, and Ru atoms, respectively.

2. Computational Strategy and Models

The formation of metal-oxide heterostructure at the nanoscale is investigated considering realistic models of titania and ruthenium systems. Specifically, we selected the $(TiO_2)_{84}$ nanoparticle (NP) because of its realistic size and bipyramidal morphology exhibiting the most stable surface of anatase crystals, and the Ru_{13} nanocluster (NC) with icosahedral symmetry, likely to be the one most stable isomer. Note that this type of metal cluster composed by 13 atoms has been systematically investigated in previous studies.[25] The stability of this, often called magic, transition metal clusters atom is due to their closed shell configuration in the spherical well potential.[26] Both $(TiO_2)_{84}$ and Ru_{13} systems are shown in **Figure 1**.

Attending to the symmetry of the $(TiO_2)_{84}$ NP, different regions are selected to anchor the Ru_{13} NC. We distinguish apical, edge, facet, and equatorial regions as reported earlier by some of us.[22] All these sites have been explicitly considered in the present study. To differentiate the sites of interaction, we have adopted the following notation: Ap, Fac, Ed, and Equat stand for apical, facet, edge, and equatorial regions, respectively. In addition, we use the digit 1 and 2 to distinguish two different sites in the same region (i.e., Fac_1 and Fac_2). Finally, the sites simultaneously having two of these terms correspond to models in which the Ru_{13} NC simultaneously interacts with these two regions. For instance, the Ed-Fac site denotes that the Ru_{13} NC is connected in the edge and facet regions. **Figure 2** shows the different configurations for the $Ru_{13}/(TiO_2)_{84}$ system.

The stability and the electronic structure of the $Ru_{13}/(TiO_2)_{84}$ nanostructures are inspected using relativistic density functional theory (DFT)-based calculations including all electrons with the electron density described through a numerical atom-centered orbital (NAO) basis set as implemented in the Fritz Haber Institute ab initio molecular simulation (FHI-aims) package.[27] To describe the properties of the $Ru_{13}/(TiO_2)_{84}$ nanostructures, the generalized gradient approximation (GGA) was selected. In particular, the Perdew–Burke–Ernzerhof (PBE) exchange-correlation density functional.[28] Nevertheless, to avoid the well-known limitations of the GGA functionals in describing the electronic structure of oxides, the final electronic structure has been analyzed by means of the PBEx hybrid functional which accurately reproduces the atomic and electronic structure of bulk rutile and anatase polymorphs of TiO_2.[29,30] A tight grid and tier-1 basis set was appropriately selected. The convergence threshold for atomic forces in relaxation of $Ru_{13}/(TiO_2)_{84}$ and isolated Ru_{13} and $(TiO_2)_{84}$ systems is set to be 10^{-3} eV Å^{-1}. Relativistic effects were included through the zero-order regular approach due to the presence of Ti and Ru, relatively heavy transition elements.[31,32]

To explore whether the formation of $Ru_{13}/(TiO_2)_{84}$ is energetically favorable, we define an energetic descriptor as the adsorption energy (E_{ads}) as

$$E_{ads} = E_{Ru_{13}/(TiO_2)_{84}} - E_{Ru_{13}} - E_{(TiO_2)_{84}} \quad (1)$$

where $E_{Ru_{13}/(TiO_2)_{84}}$, $E_{Ru_{13}}$, and $E_{(TiO_2)_{84}}$ correspond to the DFT energies of the $Ru_{13}/(TiO_2)_{84}$ nanostructures and isolated Ru_{13} NC, and $(TiO_2)_{84}$ NP, respectively. According to Equation (1), the formation of $E_{Ru_{13}/(TiO_2)_{84}}$ is exothermic and favorable when $E_{ads} < 0$.

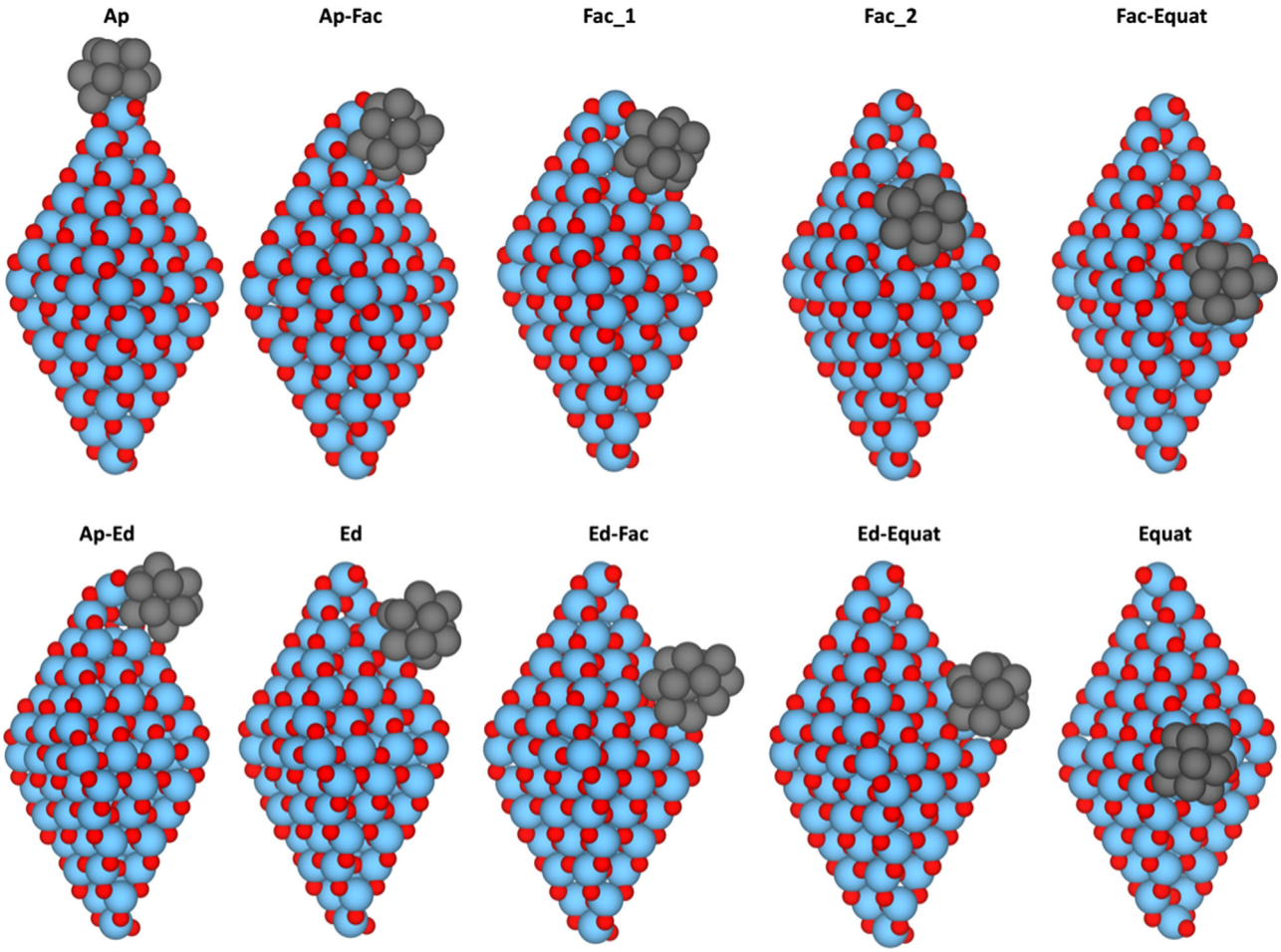

Figure 2. $Ru_{13}/(TiO_2)_{84}$ nanostructures. The adsorption energies of all these systems are listed in Table 1. Blue, red, and gray spheres correspond to Ti, O, and Ru atoms, respectively.

3. Results and Discussion

We first focus on the interaction of the Ru_{13} NC with the $(TiO_2)_{84}$ NP. Different configurations are analyzed considering the icosahedral symmetry of Ru_{13} cluster and the well-defined regions of the bipyramidal $(TiO_2)_{84}$ NP (i.e., apical, edge, facet, and equatorial). Starting with the interaction in the apical region of the $(TiO_2)_{84}$ NP, we consider two different paths to study the interacting landscape in the potential energy surface moving from the apical to the equatorial regions: i) the facet and ii) the edge routes (see Figure 2). All in all, this analysis includes ten different adsorption sites, which can be systematically reproduced due to inherent symmetry of the bipyramidal $(TiO_2)_{84}$ NP and the results derived from E_{ads} are listed in **Table 1**.

Clearly, the interaction between both nanostructures is highly exothermic, featuring E_{ads} values below −4 eV. Thus, this energetic descriptor confirms the thermodynamically favorable formation of these metal-semiconductor heterostructures. We note that this energy is calculated using exclusively the PBE density functional without including dispersion correction. Its consideration would add to a systematic extra energy around 0.2–0.3 eV. Nevertheless, preliminary tests confirm that the dispersion unalters the optimized structure obtained from PBE analysis. This is a clear indication that ionic and/or covalent character governs the interaction, being the dispersion a negligible contribution. Based on our statement, it is reasonable to focus on the PBE results as in Table 1 for further discussion and analysis.

Table 1. Adsorption energies, E_{ads}, and average coordination number, ACN of the Ru_{13} NC in $Ru_{13}/(TiO_2)_{84}$ systems. Note that ACN parameter corresponds to the Ru_{13} nanocluster. The ACN value of isolated Ru_{13} NC is also included for comparison.

Notation	E_{ads}, eV	ACN Ru_{13}
Isolated	-	6.46
Ap	−5.83	4.69
Ap-Fac	−7.09	5.92
Fac_1	−7.24	5.77
Fac_2	−6.86	5.61
Fac-Equat	−6.42	5.15
Ap-Ed	−5.16	6.15
Ed	−4.43	5.92
Ed-Fac	−6.49	5.61
Ed-Equat	−5.41	5.85
Equat	−5.59	5.54

To facilitate the discussion of the results, two different interaction routes are considered. Based on this choice, one can observe interesting results related to Ru_{13} clusters supported on the $(TiO_2)_{84}$ NP. Moving from apical to equatorial region of the $(TiO_2)_{84}$ NP through the exposed (101) facets, one notes that E_{ads} increases from −5.83 (apical) to −7.09 eV (apical-facet). Interactions slightly below −7.00 eV are systematically observed in the facet region, but its value decreases below −6.5 eV when Ru_{13} clusters are close to the equatorial region. The results obtained for the interaction in the facet regions are consistent with those reported by Pacchioni and co-authors using extended supercell models of anatase TiO_2 and a Ru_{10} NC.[18] On the other hand, the same path but through the edge region reports different results. Here, the interaction of Ru_{13} NC with $(TiO_2)_{84}$ NP is less favorable as E_{ads} decreases from a pure apical region (−5.83 eV) to a pure edge site (−4.43 eV). Then, the interaction increases up to −5.59 eV in the equatorial region. These differences are somehow expected because the interacting surface, and thus number of contacts between the interacting nanoparticles, is larger in facet than in edge regions. From this analysis, we conclude that facet regions are the most suitable sites for supported Ru_{13} NCs and edge regions, containing undercoordinated atoms and expected to be reactive, are relatively less favorable. In an intermediate situation, we find the apical region. Interestingly, two sites can be distinguished in the equatorial region, those located at the corners of the $(TiO_2)_{84}$ NP connected with the edges and the equatorial region located in the middle of two of these corners. The interaction in the first type of sites (E_{ads} = −5.59 eV) is less exothermic than in the equatorial region located in the middle of two of these corners (E_{ads} = −6.42 eV). The latter one is also the equatorial region connected with the facets of the $(TiO_2)_{84}$ NP. Similar behavior has been recently reported by some of us investigating the hydration of the $(TiO_2)_{84}$ NP with dissociative water.[22]

To rationalize the trends in E_{ads}, we select the average coordination number (ACN) of the Ru_{13} NC as a structural descriptor. Here, we note that the distorted Ru_{13} NC structures are obtaining simply relaxing the atomic structure of the initial and highly symmetrical Ru_{13} NC. The Ru_{13} NC shows ACN = 6.46 in its gas phase conformation with a highly symmetrical icosahedral shape (see Figure 1). In principle, one may assume that those interactions with large E_{ads} promote the loss of gas phase symmetry of the Ru_{13} NC reflected in the ACN parameter. Consequently, its values should be in principle below 6.46. This prediction is systematically observed as shown in Table 1. However, this descriptor is not accurate enough since no trends are observed on ACN moving from the apical to the equatorial regions of the $(TiO_2)_{84}$ NP. This indicates that other parameters in addition to the structural descriptors govern the interaction between both nanostructures. Besides, one may assume that the deformation of the Ru_{13} NC is energetically compensated by highly exothermic interaction energies. Nevertheless, the structure of the $(TiO_2)_{84}$ NP is unaltered by the presence of Ru_{13} NC. This indicates that the Ru_{13} NC induces a local effect on the titania nanostructure. To confirm this issue, we investigate the electronic properties based on the density of state (DOS) analysis.

Figure 3 shows the partial density of states (PDOS) of the $Ru_{13}/(TiO_2)_{84}$ in different situations. The PBE energy gap, E_{gap}, of the $(TiO_2)_{84}$ NP is 2.51 eV, lower than the experimental value

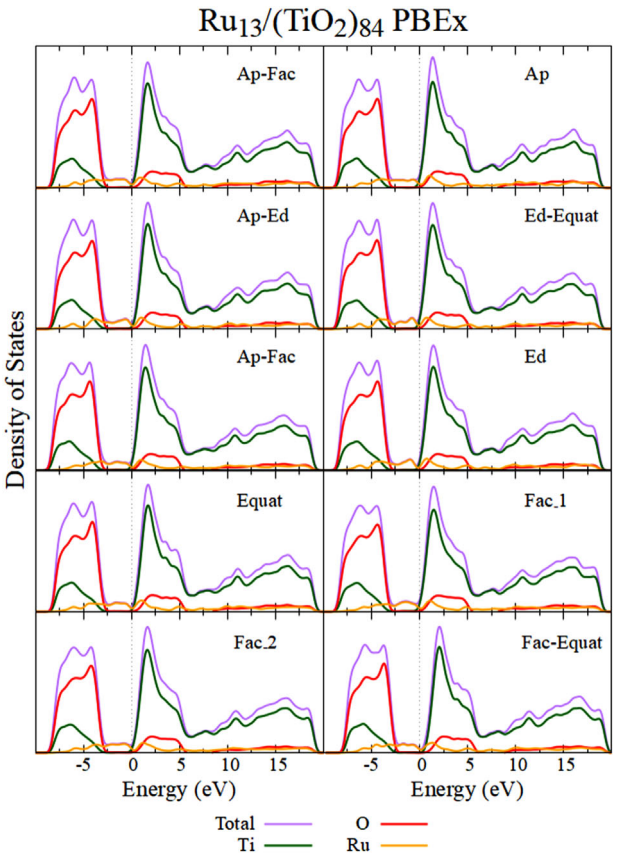

Figure 3. PBEx partial density of states (PDOS) of the $Ru_{13}/(TiO_2)_{84}$ structures depicted in Figure 2. Fermi level is fixed at 0 eV and marked with a pointed line.

of bulk anatase 3.2 eV. The value is excessively low for a nanoparticle, the energy gap is larger than that for the bulk material as evidenced in previous studies.[33,34] This discrepancy is well known and due to the limitations to GGA methods in accurately describing the electronic structure of oxides.[35,36] Including hybrid density functionals with an appropriate amount of Fock exchange can solve this issue.[35] In the particular case of TiO_2 polymorphs, a PBEx, with 12.5% Fock exchange reproduces the experimental data.[29,30] Nevertheless, while hybrids functionals open the energy gap in semiconducting materials with predicted values close to the experiment, the orbital distribution, eventually resulting in bands, is less affected. To show that this is the case also here, Figure 3 displays the PDOS of the $Ru_{13}/(TiO_2)_{84}$ structures as predicted by the hybrid PBEx whereas that arising from the PBE density functional is shown in the Supporting Information (Figure S1). The information arising from both DOS plots is qualitatively the same.

As expected, the one-electron levels of the $(TiO_2)_{84}$ NP that upon growing to the bulk will generate the valence band are dominated mainly by O 2p orbitals with a low contribution from Ti 3d orbitals regardless the density functional employed. This situation is the opposite in the levels that are related to the conduction band dominated by Ti 3d orbitals with a minimum contribution by O 2p orbitals.[37] Adding the Ru_{13} NC to the $(TiO_2)_{84}$ NP introduces a large number of Ru states within the energy gap

region so that the resulting heterostructure becomes metallic regardless the density functional (PBE or PBEx) used. This change in the electronic configuration is due to the location of the Fermi level in the conduction band like levels of the titania nanostructure. The PDOS depicted in Figure 3 shows clearly that the new states coming from Ru 4d orbitals are systematically located in the same energy region between −3 and 0 eV regardless the interaction and orientation of the Ru_{13} NC with the $(TiO_2)_{84}$ NP. In general, there are no significant differences among the investigated cases. One can see that the projection of the PDOS of Ru 4d orbitals is slightly higher in the configuration where the Ru_{13} NC is interacting mainly in facet regions than those configurations where the interaction is in the edges.

It is worth pointing out that for such a finite system, the energy levels are discrete but the energy separation becomes almost negligible and appears as a continuum in the PDOS plots in Figure 3. Interestingly, the distribution of the O and Ti states remain in similar locations relative to one another with and without the presence of the Ru_{13} NC (Figure 3). Indeed, the Ru_{13} NC interacts with only those Ti and O atoms to which it is directly bonded, leaving most states unperturbed. Thus, the energy gap of the bare $(TiO_2)_{84}$ NP does not change noticeably upon the interaction with the addition of Ru_{13} NC. This is because the new localized states, mainly of Ru(4d) character, appear in the former energy gap regions of the isolated $(TiO_2)_{84}$ NP so that, in practice, all investigated $Ru_{13}/(TiO_2)_{84}$ systems do not exhibit an electronic gap. These results can be extrapolated to other cluster and nanoparticles sizes, provide the metal NC dimension is significantly smaller than that of the oxide NP. Analogous results have been reported for the Pt_{37} NC on the (101) anatase surface.[15]

4. Conclusion

Relativistic, all electron, density functional theory-based calculations have been performed to investigate the structural and electronic properties of $Ru_{13}/(TiO_2)_{84}$ nanostructures. We conclude that the interaction between the metal cluster and semiconducting nanoparticle is highly favorable according to the calculated adsorption energies that are larger than −4 eV. We found out that the binding is more favorable in the facet regions than in the edge ones which may seem counterintuitive due to the expected larger reactivity of these regions with undercoordinated atoms but that is easily understood from the number of involved atomic contacts. This has a direct consequence on the average coordination number of the Ru_{13} NC because its deformation is larger when located in facet region. Such deformation is compensated with a highly exothermic binding energy.

The analysis of the electronic properties based on the density of states shows that the interaction is quite local because there is no significant change in the structure of $(TiO_2)_{84}$ NP, nor in the main features of its electronic structure. The contribution of 3d and 2p states of Ti and O slightly modifies once the $Ru_{13}/(TiO_2)_{84}$ nanostructure is formed. This situation is systematically observed regardless the interaction region (i.e., apical, facet, edge, or equatorial). Interestingly, the 4d states coming from Ru fill the energy gap observed in isolated $(TiO_2)_{84}$ NP promoting an almost vanishing energy gap. The contribution of such states is higher when the interaction is more exothermic.

The present results are likely to be valid for other metal clusters supported on different types of TiO_2 NPs, provides that the size of the former is significantly smaller than that of the oxide NP. The presence of the metal states would favor adsorption of photons at energies below the UV which is required for TiO_2 systems. However, the role of the metal cluster in promoting charge separations remains to be investigated and work is in progress to analyze the excited states of these systems and their time evolution.

Supporting Information

Supporting Information is available from the Wiley Online Library or from the author.

Acknowledgements

The authors acknowledge the financial support from MCIN/AEI/10.13039/501100011033 through projects PID2020-115293RJ-I00, PID2021-126076NB-I00, TED2021-129506B-C22, and the María de Maeztu MDM-2017-0767 projects with funding from FEDER *Una manera de hacer Europa*. The reported research is involved in the COST Action CA18234 (CompNanoEnergy), supported by European Cooperation in Science and Technology (COST). Computational time was provided by the *Red Española de Supercomputación* (RES).

Conflict of Interest

The authors declare no conflict of interest.

Data Availability Statement

The data that support the findings of this study are available from the corresponding author upon reasonable request.

Keywords

density functional theory, density of states, metal-semiconductor nanostructures, ruthenium nanocluster, titania nanoparticle

Received: September 13, 2022
Revised: November 3, 2022
Published online:

[1] A. Fujishima, K. Honda, *Nature* **1972**, *238*, 37.
[2] A. L. Linsebigler, G. Lu, J. T. Yates Jr., *Chem. Rev.* **1995**, *95*, 735.
[3] J. Schneider, M. Matsuoka, M. Takeuchi, J. Zhang, Y. Horiuchi, M. Anpo, D. W. Bahnemann, *Chem. Rev.* **2014**, *114*, 9919.
[4] M. Cargnello, T. Montini, S. Y. Smolin, J. B. Priebe, J. J. Delagdo Jaén, V. V. T. Doan-Nguyen, I. S. McKay, J. A. Schwalbe, M.-M. Pohl, T. R. Gordon, Y. Lu, J. B. Baxter, A. Brückner, P. Fornasiero, C. B. Murray, *Proc. Natl. Acad. Sci. USA* **2016**, *113*, 3966.
[5] G. Liu, J. C. Yu, G. Q. Lu, H.-M. Cheng, *Chem. Commun.* **2011**, *47*, 6763.
[6] J. Low, B. Cheng, J. Yu, *Appl. Surf. Sci.* **2017**, *392*, 658.
[7] J. Cai, J. Huang, Y. Lai, *J. Mater. Chem. A* **2017**, *5*, 16412.
[8] X. Cheng, C. Burda, *J. Am. Chem. Soc.* **2008**, *130*, 5018.

[9] M. Anpo, M. Takeuchi, *J. Catal.* **2003**, *216*, 505.
[10] M. Murdoch, G. I. N. Waterhouse, M. A. Nadeem, J. B. Metson, M. A. Keane, R. F. Howe, J. Llorca, H. Idriss, *Nat. Chem.* **2011**, *3*, 489.
[11] Á. Frurube, L. Du, K. Hara, R. Katoh, M. Tachiya, *J. Am. Chem. Soc.* **2007**, *129*, 14852.
[12] C. Clavero, *Nat. Photonics* **2014**, *8*, 95.
[13] P. Zhang, J. Xiong, Y. Wei, Y. Li, Y. Zhang, J. Tang, W. Song, Z. Zhao, J. Liu, *J. Catal.* **2021**, *398*, 109.
[14] L. Xiang, H. Feng, M. Liu, X. Zhang, G. Fan, F. Li, *ACS Appl. Nano Mater.* **2021**, *4*, 4688.
[15] C. L. Muhich, Y. Zhou, A. M. Holder, A. W. Weimer, C. B. Musgrave, *J. Phys. Chem. C* **2012**, *116*, 10138.
[16] D. Riassetto, C. Holtzinger, M. Langlet, *J. Mater. Sci.* **2009**, *44*, 2637.
[17] K. A. Gray, B. K. Vijayan, N. M. Dimitrijevic, J. S. Wu, *J. Phys. Chem. C* **2010**, *114*, 21262.
[18] H.-Y. T. Chen, S. Tosoni, G. Pacchioni, *J. Phys. Chem. C* **2015**, *119*, 10856.
[19] S. H. T. M. Inerbaev, D. S. Kilin, *J. Phys. Chem. Lett.* **2014**, *5*, 2823.
[20] H.-Y. T. Chen, S. Tosoni, G. Pacchioni, *ACS Catal.* **2015**, *5*, 5486.
[21] Á. Morales-García, A. Macià, F. Illas, S. T. Bromley, *Nanoscale* **2019**, *11*, 9032.
[22] L. Mino, Á. Morales-García, S. T. Bromley, F. Illas, *Nanoscale* **2021**, *13*, 6577.
[23] R. Valero, Á. Morales-García, F. Illas, *Phys. Chem. Chem. Phys.* **2020**, *22*, 3017.
[24] E. R. Remesal, Á. Morales-García, *Phys. Chem. Chem. Phys.* **2022**, *24*, 21381.
[25] S. Shetty, A. P. J. Jansen, R. A. van Santen, *J. Mol. Struct.: THEOCHEM* **2010**, *954*, 109.
[26] M. Sakurai, K. Wantanabe, K. Sumiyama, K. Suzuki, *J. Chem. Phys.* **1999**, *111*, 235.
[27] V. Blum, R. Gehrke, P. Hanke, P. Havu, V. Havu, X. Ren, K. Reuter, M. Scheffler, *Comput. Phys. Commun.* **2009**, *180*, 2175.
[28] J. P. Perdew, K. Burke, M. Ernzerhof, *Phys. Rev. Lett.* **1996**, *77*, 3865.
[29] Á. Morales-García, R. Valero, F. Illas, *Phys. Chem. Chem. Phys.* **2018**, *20*, 18907.
[30] K. C. Ko, O. Lamiel-García, J. Y. Lee, F. Illas, *Phys. Chem. Chem. Phys.* **2016**, *18*, 12357.
[31] C. Chang, M. Pelissier, M. Durand, *Phys. Scr.* **1986**, *34*, 394.
[32] E. van Lenthe, R. van Leeuwen, E. J. Baerends, J. G. Snijders, *Int. J. Quantum Chem.* **1994**, *57*, 281.
[33] D. Cho, K. C. Ko, O. Lamiel García, S. T. Bromley, J. Y. Lee, F. Illas, *J. Chem. Theory Comput.* **2016**, *12*, 3751.
[34] O. Lamiel-Garcia, K. C. Ko, J. Y. Lee, S. T. Bromley, F. Illas, *J. Chem. Theory Comput.* **2017**, *13*, 1785.
[35] I. de PR Moreira, F. Illas, R. L. Martin, *Phys. Rev. B* **2002**, *65*, 155102.
[36] Á. Morales-García, R. Valero, F. Illas, *J. Phys. Chem. C* **2017**, *121*, 18862.
[37] Á. Morales-García, S. Rhatigan, M. Nolan, F. Illas, *J. Chem. Phys.* **2020**, *152*, 244107.